Electronic Structure-Factor, Density Matrices, and Electron Energy Loss Spectroscopy of Conjugated Oligomers

V. Chernyak, S. N. Volkov, and S. Mukamel*

Department of Chemistry and Rochester Theory Center for Optical Science and Engineering, University of Rochester, P. O. RC Box 270216 Rochester, New York 14627-0216

Received: September 18, 2000; In Final Form: December 15, 2000

The electronic dynamic structure factor $S(\mathbf{q},\omega)$ of conjugated finite-size oligomers is computed using the time-dependent Hartree−Fock (TDHF) approach. The resonances observed in electron scattering are analyzed using the Bloch representation of the single-electron transition density matrices for the corresponding polymers. The separation of relative and center-of-mass motions of electron−hole pairs, which is expected to hold for infinite chains, is shown to apply even for relatively small molecules, paving the way for a band-structure picture of the quasiparticles. Signatures of the exciton coherence sizes in the momentum dependence of the structure factor are analyzed.

I. Introduction

Electronic excitations of molecules are most commonly studied by optical spectroscopies which provide a direct look at their energies and dynamics.[1] Visible and UV wavelengths are typically longer than all relevant molecular lengthscales. Consequently, the information is contained only in the frequency-dependence of the signal (e.g., absorption line shape), and the wavevector can be set to zero. This dipole approximation, which is justified by the separation of lengthscales, further results in strict selection rules that make only a very small fraction of the electronic transitions optically accessible.

The wavevector-dependence of techniques based on short-wavelength excitations such as X-ray and high-energy electron scattering carries valuable information that adds a new dimension to the frequency-profile and provides detailed information on all states including those forbidden by optical measurements. Numerous time and frequency resolved techniques are available. Recent rapid progress in X-ray[2−8] and electron pulse generation[9−12] had opened up new possibilities for coherent short wavelength measurements. A similar state of affairs exists in vibrational spectroscopy where wavevector-dependent neutron scattering[13] eliminates the selection rules of infrared and Raman optical techniques.

In this article, we focus on frequency-domain electron energy loss spectroscopy (EELS), which constitutes a powerful tool for the studies of electronic excitations in molecules.[14] The approach may be, however, directly applied to time-resolved X-ray and electron scattering measurements. In an EELS experiment, hundreds keV electrons are scattered off a thin (∼100 nm) film of the studied material. The deflected electrons change their momentum and energy from $\mathbf{k}_i$, ϵ_i to $\mathbf{k}_f$, ϵ_f. The inelastic scattering cross-section is measured vs the electron-energy loss $\omega \equiv \epsilon_i - \epsilon_f$ and momentum change $\mathbf{q} \equiv \mathbf{k}_i - \mathbf{k}_f$. The resonances in the few eV range correspond to the low-energy electronic excitations. The energy loss is typically $\sim 10^5$ times smaller than the incident electron energy. Wavevectors of the electronic excitations of interest lie in the region up to 1 $Å^{-1}$, which means that the momentum $\mathbf{q}$ transferred from an incident electron to a molecule is small, and electron deflection angles are of the order of a few milliradians. The frequency and wavevector-dependent electron-scattering cross-section is[14]

$$\frac{d\sigma}{d\Omega} \propto \frac{1}{q^4} S(\mathbf{q},\omega) \tag{1.1}$$

where the dynamic structure factor $S(\mathbf{q},\omega)$ is the Fourier transform of the density−density correlation function:

$$S(\mathbf{q},\omega) = \frac{1}{2\pi\hbar N} \int dt \langle \tilde{n}(\mathbf{q},t)\tilde{n}(-\mathbf{q},0)\rangle \exp(-i\omega t) \tag{1.2}$$

N is the number of electrons in the sample, and $\tilde{n}(\mathbf{q},t)$ is the Fourier transform of the electronic-density operator in the Heisenberg representation:

$$\tilde{n}(\mathbf{q},t) \equiv \int d\mathbf{r}\, \tilde{n}(\mathbf{r},t) \exp(i\mathbf{q}\cdot\mathbf{r}) \tag{1.3}$$

EELS spectra in a variety of conjugated organic molecules[15−17] have been interpreted in terms of the $\mathbf{q}$ dependence of the lowest-peak integrated intensity. The characteristic peak width has been associated with the inverse exciton size. However, the relation between the EELS spectra and the exciton size is not straightforward, since, due to the momentum conservation, the transferred momentum in the EELS is related to the center-of-mass momentum of the created exciton rather than to the parameters of the relative motion of an electron and a hole.[28]

In this paper, we apply a time-dependent algorithm based on the electronic density matrix for computing the dynamic structure factor. $S(\mathbf{q},\omega)$ is expressed as the linear response to an external potential E coupled to the electron density, and closed expressions for the EELS signal are derived in terms of the eigenmodes of the linearized time-dependent Hartree−Fock (TDHF) equation,[18] known as the collective electronic oscillators (CEO).[19,20] Our analysis can be directly extended to time-dependent density functional theory (TDDFT), which is formally equivalent to the TDHF.[21]

In section II, we derive closed expressions for the dynamic structure factor $S(\mathbf{q},\omega)$ using the TDHF. Details of the derivation are given in Appendix A. In section III, we present numerical calculations for elongated carotenoids of different sizes and for

* To whom correpondence should be addressed.

10.1021/jp0033465 CCC: $20.00
Published on Web 02/17/2001

a *p*-phenylene vinylene (PPV) oligomer. Our calculations demonstrate that the band picture that is asymptotically exact for polymers is still valid for surprisingly short oligomers, with, for example, $N = 10$ repeat units. This is in good agreement with recent experiments showing a quasi-band-structure for relatively short oligomers.[22,23]

In Appendix B, we apply the band theory to characterize the CEO modes in infinite polymer chains. These will be used for the interpretation of the oligomer calculations. We derive an equation that allows one to find the CEO (exciton) bands and compute the structure factor and the EELS signals. This derivation is based on the INDO approximation, which is also used in our numerical calculations for finite-size molecules. The infinite-chain results are used in section III for identifying polymer-specific features in finite-size oligomers. Classification of electronic modes into quasi-bands is rather clear in longer chains, as illustrated by contour plots representing the structure of the modes. However, this further gives an intuitive way for classifying the modes even in shorter oligomers where the quasi-band structure is not so obvious a priori.

In Appendix D, we derive a simple approximate expression for $S(\mathbf{q},\omega)$ for infinite polymers using a simplified PPP-like Hamiltonian. This uses the linearized TDHF equation in the molecular-orbital representation developed in Appendix C. Using the results of Appendices C and D, we discuss in section IV the possibility of extracting information related to exciton size from EELS measurements. Specifically, we show that even though the width of the momentum dependence of the lowest inelastic peak in the spectrum may not be associated with the exciton size, it still provides an indirect measure of the momentum dependence of that size.

II. TDHF Calculation of the Dynamical Structure Factor

We assume that the electronic-density operator $\hat{n}(\mathbf{r})$ is coupled to an external time-dependent potential $E(\mathbf{r},\tau)$ by an interaction Hamiltonian

$$\hat{H}_{\text{int}}(\tau) \equiv -\int d\mathbf{r} E(\mathbf{r},\tau)\hat{n}(\mathbf{r}) \tag{2.1}$$

By expanding the expectation value of the Heisenberg electronic-density operator $\tilde{n}(\mathbf{r},\tau)$ to first order in the potential we have

$$\langle \tilde{n}(\mathbf{r},\tau)\rangle = \int_0^\infty dt R(t;\mathbf{r},\mathbf{r}')E(\mathbf{r}',\tau - t) \tag{2.2}$$

where R is the density−density response function:

$$R(t;\mathbf{r},\mathbf{r}') = \frac{i}{\hbar}\langle[\tilde{n}(\mathbf{r},t), \tilde{n}(\mathbf{r}',0)]\rangle \tag{2.3}$$

In the frequency domain, we define the linear density−density polarizability

$$\alpha(\omega;\mathbf{r},\mathbf{r}') \equiv \int_0^\infty dt R(t;\mathbf{r},\mathbf{r}')\exp(i\omega t) \tag{2.4}$$

In Appendix A, we show that the dynamic structure factor $S(\mathbf{q},\omega)$ may be expressed in terms of $\alpha(\omega;\mathbf{r},\mathbf{r}')$:

$$S(\mathbf{q},\omega) = 2\,\text{Im}[\int d\mathbf{r}d\mathbf{r}'\alpha(\omega;\mathbf{r},\mathbf{r}')\exp[i\mathbf{q}\cdot(\mathbf{r}-\mathbf{r}')]] \tag{2.5}$$

$\alpha(\omega;\mathbf{r},\mathbf{r}')$ can be computed using the TDDFT or the TDHF approaches.

The linearized TDHF Liouville-space operator L that defines the eigenmodes (collective electronic oscillators) ξ_α through the eigenvalue problem $L\xi_\alpha = \Omega_\alpha\xi_\alpha$ is given by:[19,20]

$$L\xi = [t + V\bar{\rho},\xi] - [\bar{\rho},V\xi] \tag{2.6}$$

where t is the hopping matrix, V is the tetradic operator representing the Coulomb interactions, and $\bar{\rho}$ is the ground-state density matrix. Using an orthogonal and real basis set of single-electron atomic orbitals $\varphi_m(\mathbf{r})$, the TDHF response function assumes the form:

$$\alpha(\omega;\mathbf{r},\mathbf{r}') = \sum_v\left\{\frac{\text{Tr}[\mu(\mathbf{r})\xi_v^\dagger]\text{Tr}[\mu(\mathbf{r}')\xi_v]}{\omega + \Omega_v + i\Gamma} - \frac{\text{Tr}[\mu(\mathbf{r})\xi_v]\text{Tr}[\mu(\mathbf{r}')\xi_v^\dagger]}{\omega - \Omega_v + i\Gamma}\right\} \tag{2.7}$$

where ξ_v are the eigenmodes of the linearized TDHF equation with positive frequencies Ω_v, Γ is a dephasing rate, and $\mu(\mathbf{r})$ is a matrix in the single-electron space with matrix elements

$$\mu_{mn}(\mathbf{r}) = \varphi_m(\mathbf{r})\varphi_n(\mathbf{r}) \tag{2.8}$$

Substituting eq 2.7 into eq 2.5 finally yields

$$S(\mathbf{q},\omega) = \sum_v|\text{Tr}[\bar{\mu}(\mathbf{q})\xi_v^\dagger]|^2\frac{2\Gamma}{(\omega - \Omega_v)^2 + \Gamma^2} \tag{2.9}$$

with

$$\bar{\mu}_{mn}(\mathbf{q}) \equiv \int d\mathbf{r}\varphi_m(\mathbf{r})\varphi_n(\mathbf{r})\exp(-i\mathbf{q}\cdot\mathbf{r}) \tag{2.10}$$

Equations 2.9 and 2.10 express the dynamic structure factor in terms of the single-electron orbitals and the eigenmodes of the linearized TDHF equations. The linear optical absorption line shape is given by the $q \to 0$ limit of these equations, since the first nonvanishing term in the power series expansion of $\text{Tr}[\bar{\mu}(\mathbf{q})\xi_v^\dagger]$ at small q is proportional to the expectation value of the dipole moment. Selection rules greatly restrict the number of optically accessible transitions. In contrast, the **q**-dependent EELS signals probe the entire band of excitations. It should be noted that these results apply for arbitrary molecular geometry and translational invariance was not assumed.

The CEO modes represent the joint motion of electron−hole pairs. For periodic structures such as infinite polymers, they can be factorized into the relative-motion and the center-of-mass contributions. The latter have the particle-in-a-box wave functions characterized by a momentum **q** which becomes a good quantum number. The modes and their frequencies thus become momentum-dependent and the molecular dynamic structure factor per unit cell can be recast in the form (see Appendix B):

$$S(\mathbf{q},\omega) = \sum_v|\text{Tr}[\tilde{\mu}(\mathbf{q})\tilde{\xi}^{(v)\dagger}(\mathbf{q}\cdot\mathbf{R})]|^2\frac{2\Gamma}{[\omega - \Omega^{(v)}(\mathbf{q}\cdot\mathbf{R})]^2 + \Gamma^2} \tag{2.11}$$

where $\tilde{\mu}(\mathbf{q})$, $\tilde{\xi}^{(v)\dagger}(\mathbf{q}\cdot\mathbf{R})$, and $\Omega^{(v)}(\mathbf{q}\cdot\mathbf{R})$ are the Bloch representation for the dipole-moment operator and for the eigenmode and an eigenvalue of the Liouville equation for the infinite periodic molecule, respectively. **R** is the lattice vector representing the displacement between neighboring unit cells. Closed expressions for all of these quantities are given in Appendix B.

Band structure is commonly used to describe the motion of a single quasiparticle (an electron, a hole, or Frenkel exciton) in a periodic potential, using the Bloch theorem. Here we consider a composite quasiparticle (exciton) whose center-of-

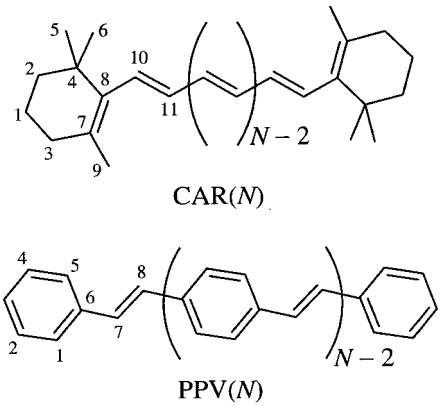

Figure 1. Molecular geometry and atom numbering for an elongated carotenoid CAR(*N*) and a PPV oligomer PPV(*N*) with *N* repeat units.

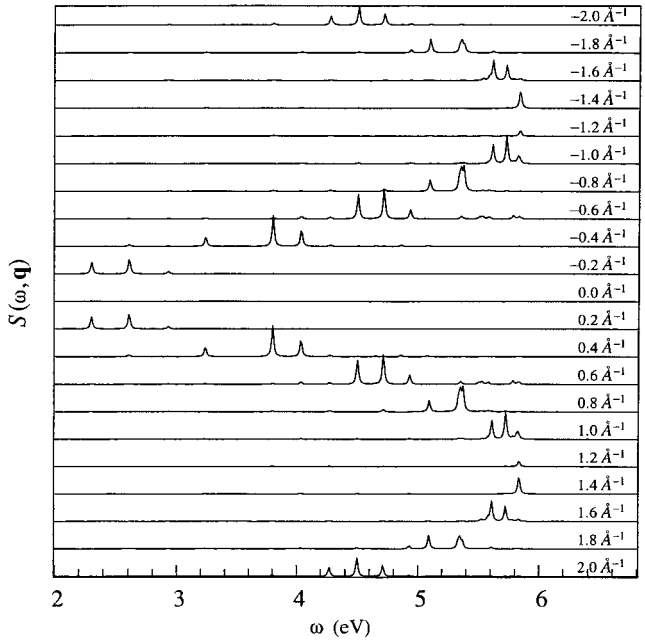

Figure 2. Calculated dynamic structure factor $S(\mathbf{q},\omega)$ (eq 2.9) of CAR(20) plotted vs the energy loss ω for different momentum transfer **q** parallel to the molecular axis and $\Gamma = 0.01$ eV.

mass motion is described as a particle-in-a-box and the relative motion is quantized, with different states forming different bands. Let us compare eqs 2.9 and 2.11 for a molecule with *M* electrons and *N* repeat units, each described by a basis set of *K* orbitals. In eq 2.9, $\bar{\mu}$ and ξ_ν are $NK \times NK$ matrixes. There are altogether $N_\nu = (NK - M)M$ positive-frequency modes $\nu = 1, ..., N_\nu$ and the ξ_ν matrices are of rank N_ν. In eq 2.11, we have a different structure. $\tilde{\xi}^{(\nu)}$ have only NK^2 distinct elements ($K \times K$ matrices that depend on *N*). Each element is a function of **q** and there are *N* values of **q**. Each $\Omega^{(\nu)}(\mathbf{q}\cdot\mathbf{R})$, $\tilde{\xi}^{(\nu)}(\mathbf{q}\cdot\mathbf{R})$ for a given ν and varying values of **q** form a band.

III. CEO Modes and Structure Factor in Elongated Carotenoids and PPV Oligomers

We have computed $S(\mathbf{q},\omega)$ for three elongated carotenoids [CAR(*N*)] with $N = 10$, 20, and 40 repeat units; [CAR(10) resembles the natural β-carotene]. We further considered an oligomer of *p*-phenylene vinylene PPV(10) (see Figure 1).

In an infinite polymer chain, the dynamic structure factor $S(\mathbf{q},\omega)$ (eq 2.11) has resonance peaks at $\omega = \Omega^{(\nu)}(\mathbf{q}\cdot\mathbf{R})$. $\Omega^{(\nu)}$ form distinct bands labeled by the band index ν. The following calculations show that the maxima of $S(\mathbf{q},\omega)$ (eq 2.9) form bands $\omega(\mathbf{q})$ even in medium-size oligomers, with the difference that

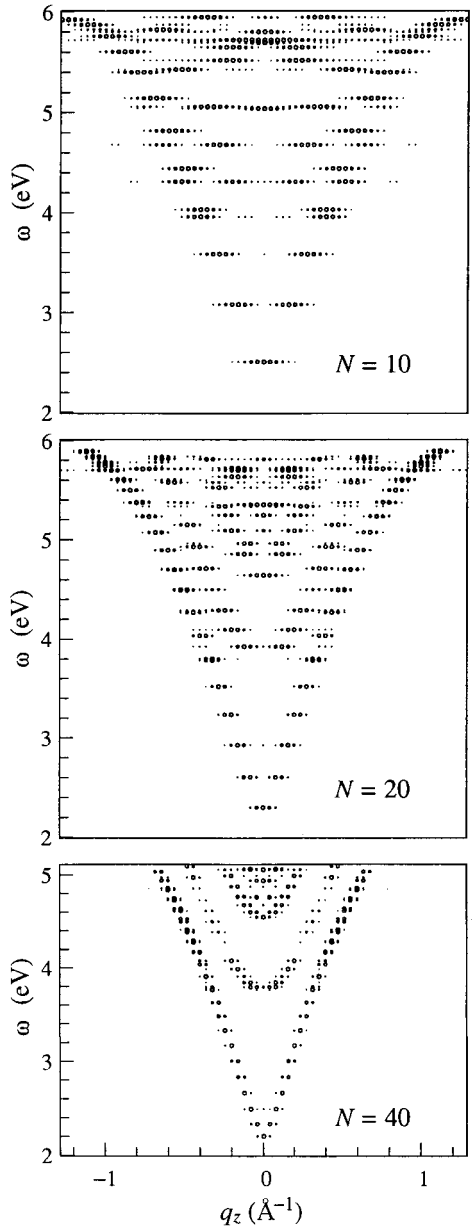

Figure 3. Calculated $S(\mathbf{q},\omega)/q^2$ for **q** directed along the molecular axis and $\Gamma \to 0$. Each CEO mode gives a series of peaks at frequency $\omega = \Omega_\nu$ but with different values of **q**. The radius of each circle is proportional to the peak intensity. Normalization for each frequency (horizontal lines) is performed for clarity. (For translationally invariant system, each CEO mode will give a single peak at a particular value of **q**.) Top panel: 26 lowest-frequency electronic modes of CAR(10); middle panel: 50 lowest modes of CAR(20); bottom panel: 50 lowest modes of CAR(40).

the CEO mode frequencies Ω_ν can only assume discrete **q**-independent values. The appearance of a distinct band structure, characteristic of infinite polymer chains, even for small oligomers, indicates an approximate factorization of the electron−hole relative and center-of-mass motions. This is further confirmed by the following 2D plots of the collective electronic oscillators which show a separation of the diagonal (center-of-mass) with the off-diagonal (relative) motions.

Ground-state geometries optimized at the AM1 level using *Gaussian94*[24] were taken from ref 20. We used the INDO/S semiempirical Hamiltonian, as parametrized by Zerner and co-workers in the ZINDO code.[25,26] The ground-state Hartree−Fock single-electron density matrix $\bar{\rho}_{mn}$ was computed, and the eigenmodes $\xi_{\nu,mn}$ of the linearized TDHF equation (eq 2.6) were

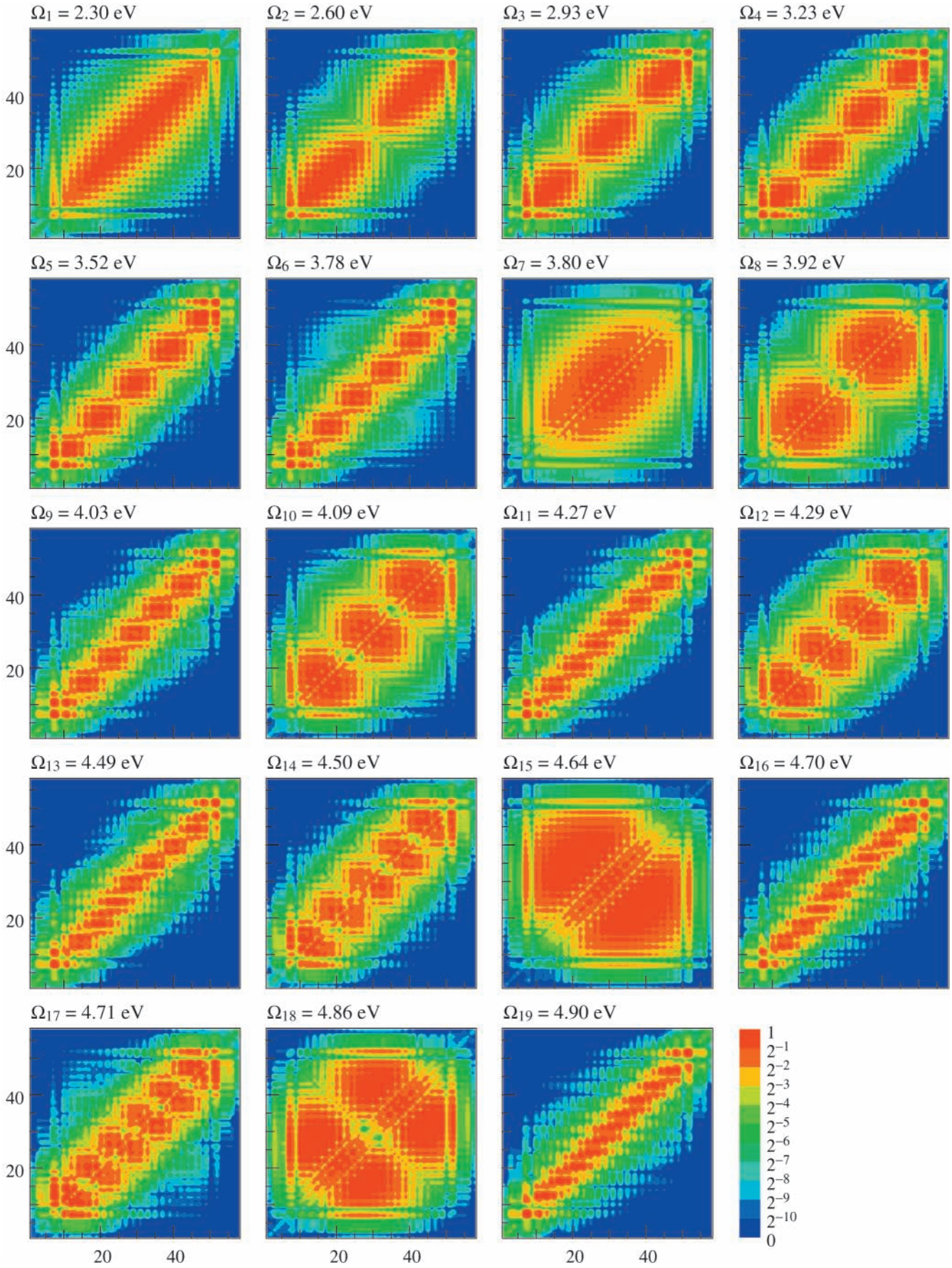

Figure 4. Lowest-frequency modes $\xi_{\nu,nm}$ of CAR(20) plotted on a logarithmic scale. The *x* and *y* axes are labeled by the carbon atoms to which the *m*th or *n*th atomic orbitals belong. Mean-square averaging is performed over all pairs of *m*th and *n*th atomic orbitals corresponding to each particular pair of atoms (see ref 29). The carbon atom numbering is given in Figure 1. Shown are the lowest 19 modes.

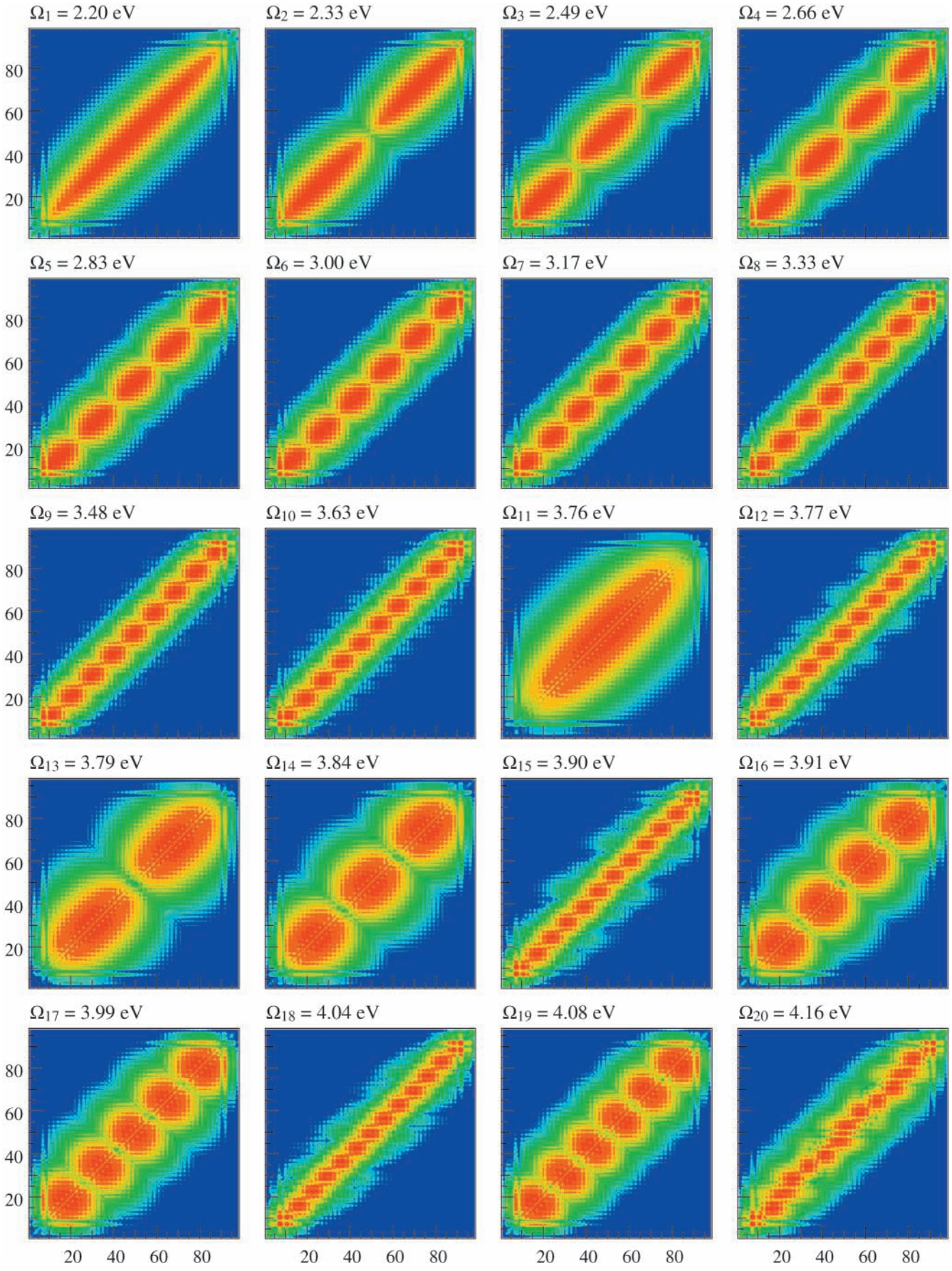

Figure 5. The lowest 50 modes of CAR(40). For details see Figure 4.

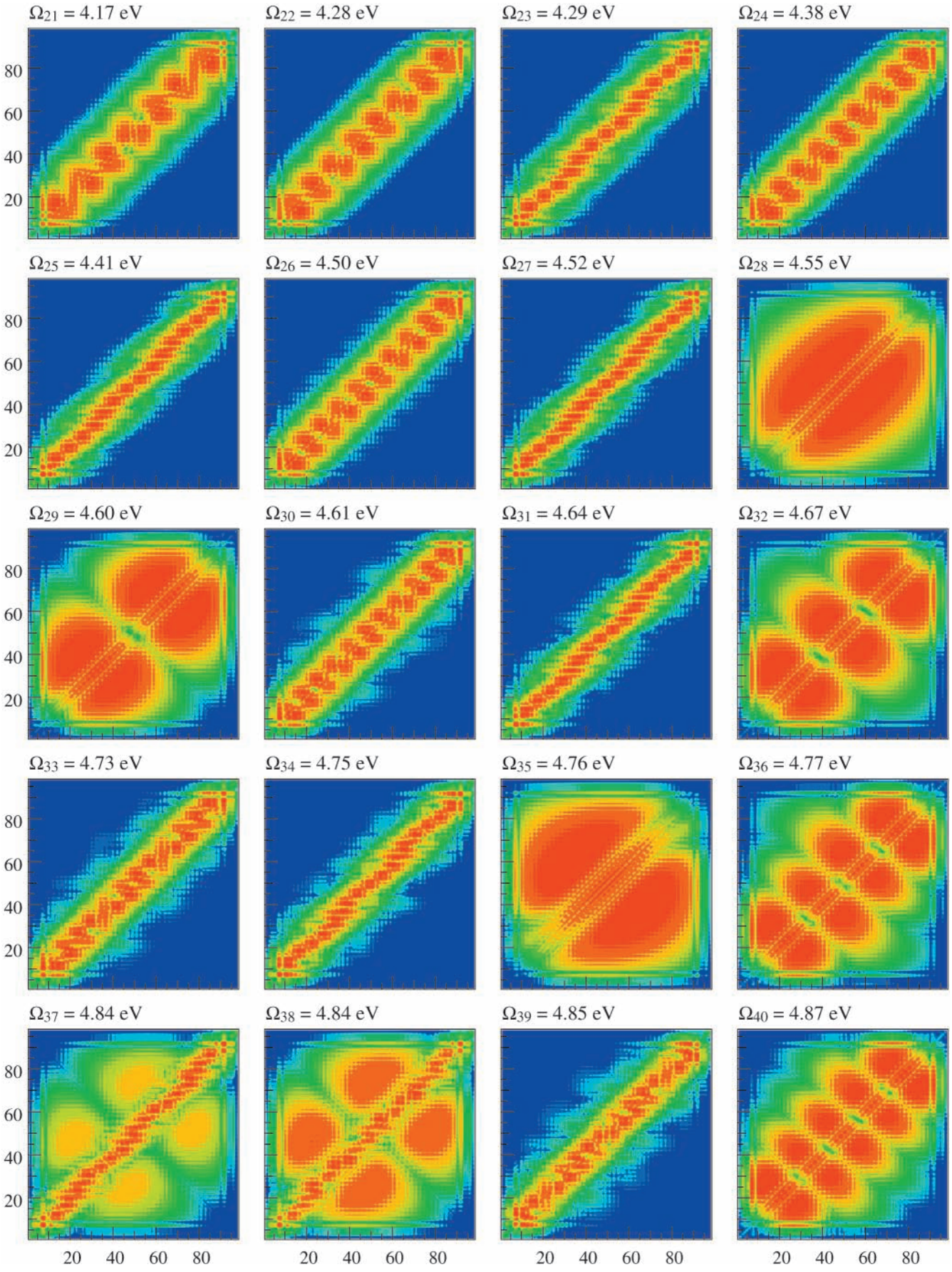

Figure 5 (continued)

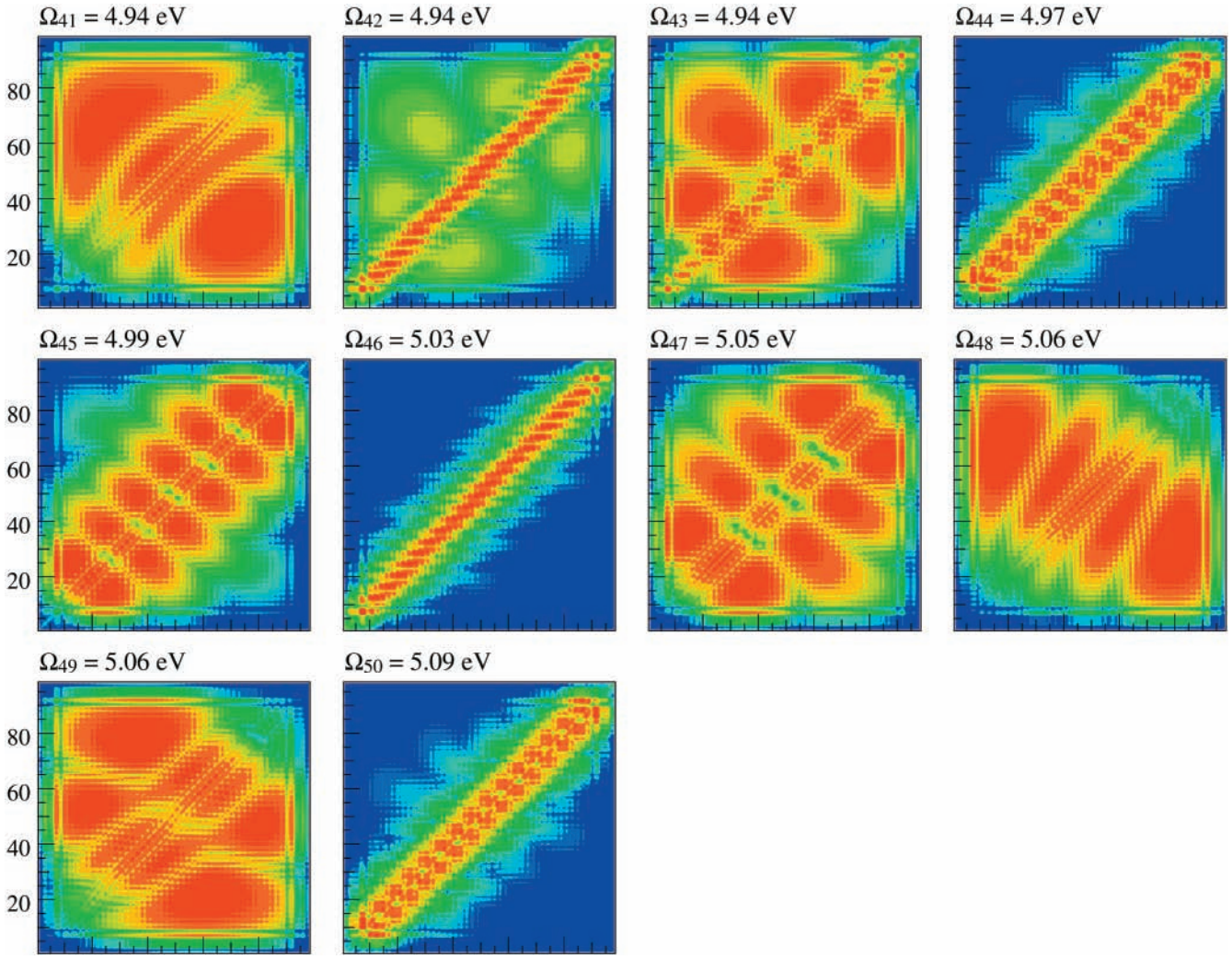

Figure 5 (continued)

then obtained using the oblique Lanczos algorithm.[27] $S(\mathbf{q},\omega)$ (eq 2.9) was computed using 50 lowest-frequency CEO modes $\xi_{\nu,mn}$. In all calculations, **q** was directed along the molecular axis. The momentum-space electron density $\mu_{mn}(\mathbf{q})$ was calculated using eq 2.10, neglecting the overlap of electronic orbitals centered at different atoms, and expanding the exponential factor to first order in **r** around the center of the atom to which a particular atomic orbital belongs.

Figure 2 depicts the variation of the frequency-dispersed $S(\mathbf{q},\omega)$ of CAR(20) with **q**. We note that the largest peaks of $S(\mathbf{q},\omega)$ for each ω form a curve $q(\omega)$ that shows approximate periodicity with period $\approx$2.6 Å^{-1}. This is in good agreement with the half-width π/R of the Brillouin zone of the corresponding polymer where the lattice constant is $R \approx 2.45$ Å.

In Figure 3 we display $S(\mathbf{q},\omega)/q^2$ which is proportional to the EELS signal vs **q** and ω for CAR(10), CAR(20), and CAR(40) in a different format. We divide by q^2 because it follows from eqs 2.9 and 2.10 that $S(\mathbf{q},\omega) \propto q^2$ for $q \rightarrow 0$ [cf. also eqs D17 and D19]. The values of $S(\mathbf{q},\omega)/q^2$ are normalized separately for each ω to best illustrate the q-dependence for each CEO mode; the relative oscillator strengths of the modes depicted in Figure 2 are thus not shown. Each CEO mode has resonances at different values of q represented by circles whose radii are proportional to the peak intensities. The range of q in Figure 3 roughly covers the first Brillouin zone of the infinite polymer chain. The figure demonstrates how the band structure of elongated carotenoids becomes more pronounced with increasing N where the CEO modes form a more dense manifold. Three lowest bands with band-edges at $\approx$2.2, $\approx$3.8, and $\approx$4.6 eV are clearly identified for CAR(20) and CAR(40).

Many CEO modes can be assigned to a particular band according to the location of the maxima in the **q** dependence of $S(\mathbf{q},\omega)$ at $\omega = \Omega_\nu$ using Figure 3. However, for frequencies higher than the second band-edge, we find that modes from different bands but with close frequencies may be mixed. In this case, Figure 3 may not be sufficient for a unique classification of the modes.

The bands and CEO modes can be further characterized using 2D contour plots of the single-electron transition density matrixes $\xi_{\nu,mn}$. Figure 4 shows $\xi_{\nu,mn}$ for the 19 lowest-frequency modes of CAR(20), with the axes labeled by the carbon atoms to which the mth (nth) atomic orbitals belong (Figure 1). The plots span 3 orders of magnitude on a logarithmic scale from red (large) to blue (small), with the absolute values of $\xi_{\nu,mn}$ normalized to the maximum. Comparing Figures 3 and 4 shows that the number of nodes (or peaks) in the antidiagonal direction in the 2D plot of $\xi_{\nu,mn}$ is fixed for a given band, while in the diagonal direction the number increases with q within the same band. This suggests that the relative and center-of-mass motions of the electron−hole pairs are virtually independent, i.e., $\xi_{\nu,mn}$ may be factorized as expected for infinite polymer chains (eq B3).

It is clearly seen from Figure 4 that the $\nu = 1-6$, 9, 11, 13, 16, 19 modes have a single peak in the antidiagonal direction

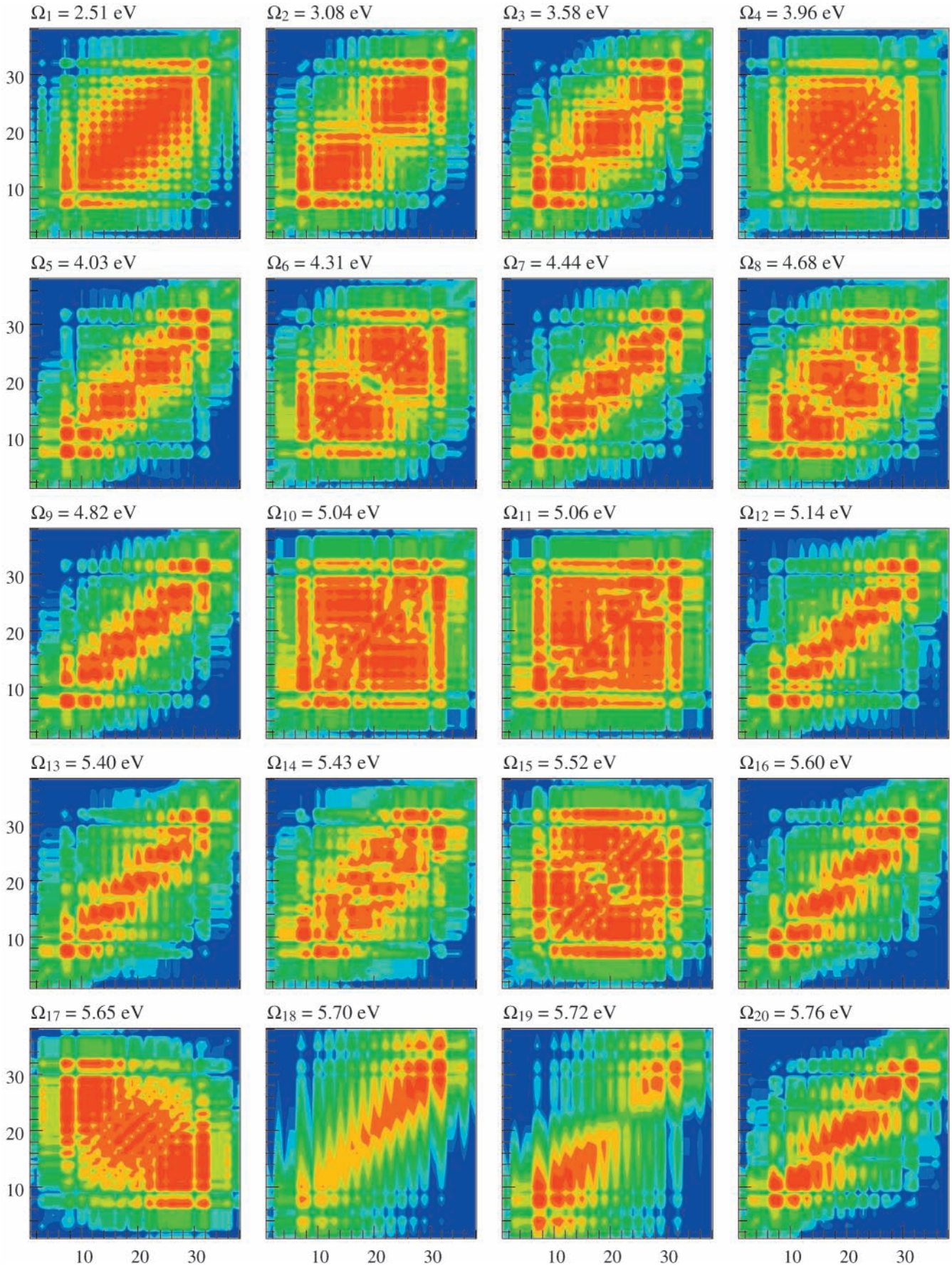

Figure 6. The lowest 50 modes of CAR(10). For details see Figure 4.

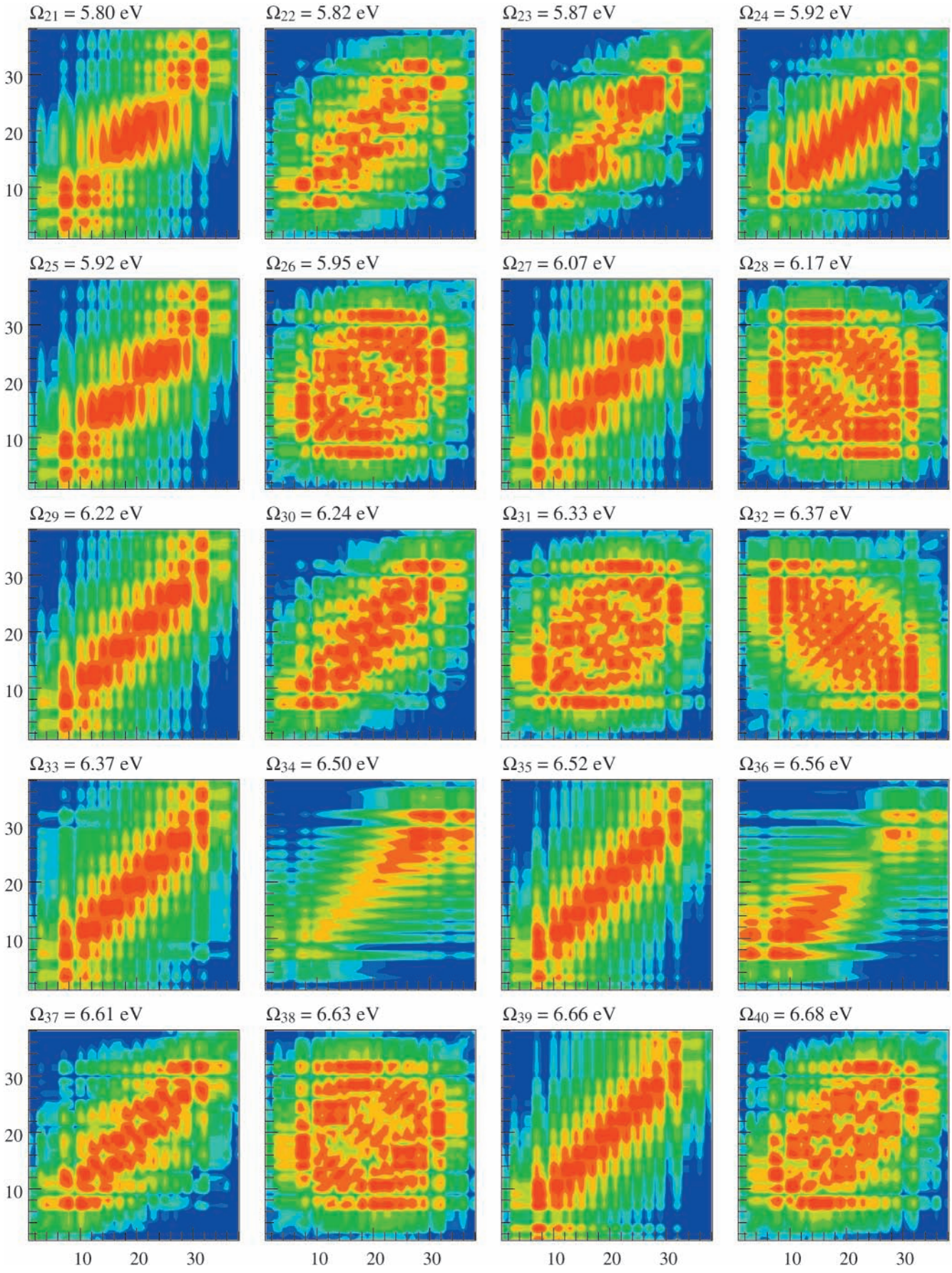

Figure 6 (continued)

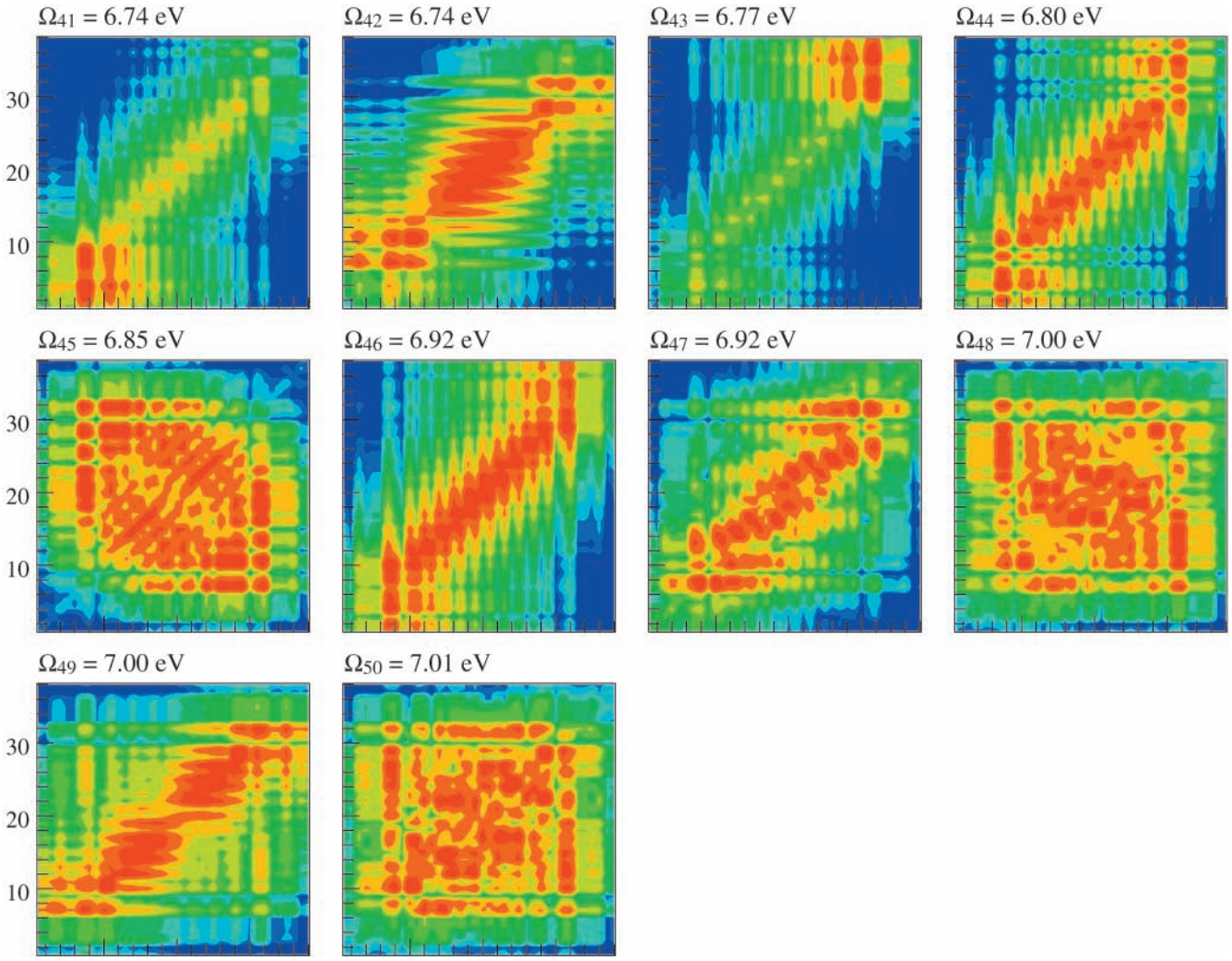

Figure 6 (continued)

and thus belong to the first band. The number of peaks along the diagonal direction uniquely distinguishes the various modes of the first band; this number characterizes the momentum of the exciton's center of mass, resembling a particle in a 1D box. The higher the momentum, the more peaks and nodes are found in the diagonal direction, and the higher the frequency of the mode. The $\nu = 7, 8, 10, 12, 14, 17$ modes have two peaks in the antidiagonal direction, indicating that they belong to the second band where a different pattern of the particle−hole relative motion is realized. The $\nu = 15$ and 18 modes belong to the third band and have three peaks in the antidiagonal direction.

The band structure of the CEO modes becomes more sharply defined for longer oligomers where edge effects are less pronounced and the separation of the particle−hole center-of-mass and relative motions is more justified. This is illustrated for CAR(40) in Figure 5. Modes from the six lowest-frequency bands are easily recognizable among the 50 lowest modes shown. Comparing the modes of CAR(20) and CAR(40), we note that the frequency of a mode belonging to a particular band is mainly determined by the distance between the nodes in the diagonal direction ("particle-in-the-box" motion). For instance, in the lowest band the frequencies of the first, second, and third modes for CAR(20) (2.30, 2.60, and 2.93 eV) are close to those of the second, fourth, and sixth modes for CAR(40) (2.33, 2.66, and 3.00 eV, respectively) that correspond to the distances between nodes of 20, 10, $6^2/_3$ repeat units (neglecting the end groups). In the second band, the frequencies of the first, second, and third modes for CAR(20) (3.80, 3.92, and 4.09 eV) almost coincide with those of the second, fourth, and sixth modes of the second band for CAR(40) (3.79, 3.91, and 4.08 eV, respectively), as well as the internode distances. It then follows that we can view the $(2n)$th mode in a particular band for CAR(40) as a combination of two nth modes in the same band for CAR(20), with negligible interaction between them. The density of states of CAR(40) is thus almost twice that of CAR(20).

Once two or more modes from different bands mix, they may no longer be rigorously assigned to a particular band. Nevertheless, they can be effectively described by taking into account the exciton scattering effects at the ends of the molecule. However, provided exciton scattering is not too strong, we can still approximately assign the mode to one of the bands according to the node structure of its transition density matrix. For example, the $\nu = 6$ mode in Figure 4 has a small component of the first mode from the second band, but the main contribution is definitely from the sixth mode of the first band. The pairs of modes 37, 38, and 42, 43 in Figure 5 are good examples of strong mixing of nearly degenerate modes from the first and fourth bands.

Understanding the classification of bands and CEO modes for relatively long oligomers should help identify the same pattern for smaller carotenoids such as CAR(10) (Figure 6) which is closer to the natural β-carotene molecule. Since the

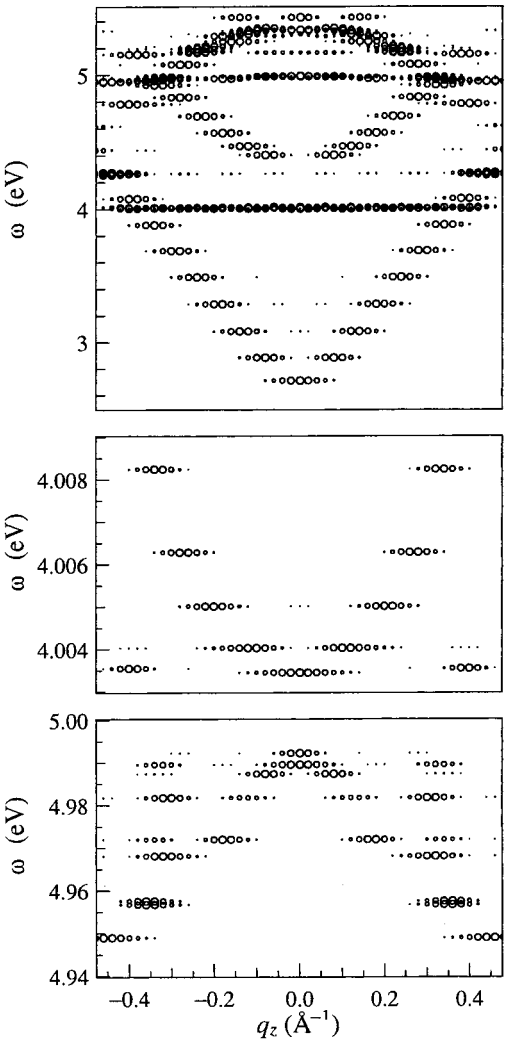

Figure 7. Top panel: same as Figure 3 but for 50 lowest-frequency modes of PPV(10) ($\Gamma \rightarrow 0$). The middle and bottom panels show the two "flat" bands of the top panel on an expanded frequency scale. Their frequency dispersion is 2−3 orders of magnitude smaller than for the other bands.

mode frequency spacing is twice that of CAR(20), we have more bands in the frequency range of the lowest 50 modes and a wider variety of mode types. Mixing of modes belonging to different bands complicates the mode classification at high frequencies. An interesting feature of the modes at the top of a band is that the number of nodes in the diagonal direction increases as the frequency is lowered from the upper band-edge, which is similar to the behavior near the lower band-edge. This is clearly seen in Figure 6 where the 24, 23, 20, 16, 13, ... modes form the top of the first band. We further see modes from new bands (not shown in Figure 3) which have no nodes in the antidiagonal direction, like the modes from the first band. However, the pattern of the electronic excitation in the unit cell is markedly different (see e.g., the modes with $\upsilon = 21$ and 25).

We have also calculated the 50 lowest-frequency CEO modes for the *p*-phenylene vinylene PPV(10) (Figure 1). This oligomer has a richer band structure compared to carotenoids. The top panel of Figure 7 displays $S(\mathbf{q},\omega)/q^2$, in the same way as in Figure 3. The momentum transfer $\mathbf{q}$ is again directed along the molecular axis. The range of q in Figure 7 corresponds to the first Brillouin zone. We can distinguish several bands, some have their top at $q = 0$. There is a flat band in the frequency region around 4 eV with the effective exciton mass almost 3 orders of magnitude less than for the first band. (The effective exciton mass was estimated at $q \approx 0$ based on the curvature of the quasi-band at that point.) Another flat band lying just below 5 eV is concave (i.e., has the maximum-frequency mode at $q = 0$) with exciton effective mass 2 orders of magnitude less than the first band. In these bands, the atoms bridging the phenyl rings weakly participate in the excitation while the induced density matrix still shows coherences between the phenyl rings and between the phenyl rings and these bridges. These two bands are displayed on an expanded frequency scale in the middle and bottom panels of Figure 7.

Most of the 50 lowest-frequency CEO modes for PPV(10) shown in Figure 8 can be easily assigned to a specific band in Figure 7. However, for frequencies $\omega \geq 5$ eV mode mixing belonging to different bands makes such classification more difficult. We further note that besides the number of nodes in the antidiagonal direction, the CEO modes belonging to different bands may be distinguishable by the electronic excitation pattern, as was demonstrated for short carotenoids in Figure 6.

Discussion

We have recently demonstrated that for intermediate-size molecules where spectral resolution is high and the EELS peaks related to different excitons are well resolved, the momentum dependence of the lowest peak integrated intensity only carries information on the molecule size.[28] Additional information on the dependence of the exciton size on its momentum may be extracted from the relative integrated intensities of the higher EELS peaks. It is, however, sometimes possible to extract meaningful information on exciton properties from the momentum dependence of the lowest peak intensity. This is the case for sufficiently long oligomers where exciton lines overlap. The lowest peak then represents many overlapping excitons, rather than the lowest-energy one. The momentum dependence of this collective peak provides information on the higher-momentum excitons. The situation becomes very clear in infinite polymers where the exciton momentum is a good quantum number and the lowest peak in the spectrum is represented by the lowest exciton with a given momentum (i.e., the exciton from the lowest band) rather than by the absolutely lowest-energy exciton.

To gain insight into the behavior of $S(\mathbf{q},\omega)$ in this limit, we consider a simple model of an infinite polymer chain with two orbitals per unit cell and a simplified Pariser−Parr−Pople (PPP) type Hamiltonian. This model, which describes qualitatively the π-orbitals of an elongated carotenoid, is analyzed in Appendix D for the limit of weak bond alteration, whereby the bond alternation parameter (eq (D1)) $\zeta \ll 1$, and weak Coulomb interaction when the exciton size $l_e \gg \zeta^{-1}$. In this case the problem may be reduced to a 1D particle on a lattice. The electronic eigenmodes are expressed in terms of the particle wave function (eqs C4, D8, D13, and D14). The calculation is based on the effective mass approximation and neglecting processes that do not conserve the number of electron−hole pairs. Both assumptions are valid when $l_e \gg \zeta^{-1}$.

It follows from eqs D17, D19, and D14, that the integrated EELS signal

$$I(\mathbf{q}) \equiv \frac{1}{(\mathbf{q}\cdot\mathbf{R})^2}\int \frac{d\omega}{2\pi} S(\mathbf{q},\omega) \tag{4.1}$$

can be expressed as a product of two factors:

$$I(\mathbf{q}) = \frac{1}{\zeta^2 + s^2}|g(0;s)|^2 \tag{4.2}$$

where $s = \mathbf{q}\cdot\mathbf{R}$. The first factor shows the change of the structure factor on a typical momentum scale $s \sim \zeta$ related to the bond

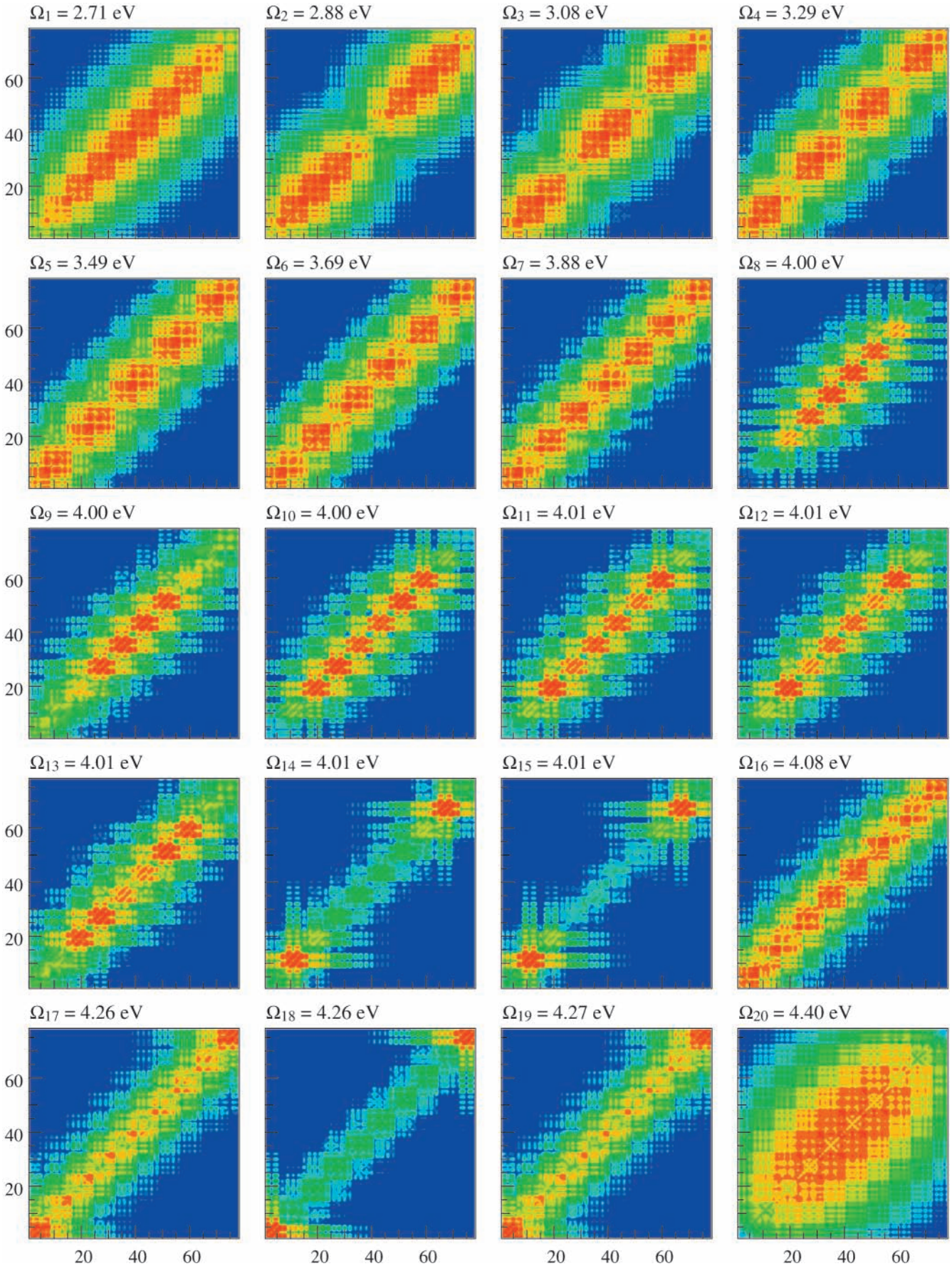

Figure 8. Fifty lowest-frequency modes $\xi_{\nu,mn}$ of the PPV(10) (see caption to Figure 4 for details). The carbon atoms numbering is given in Figure 1.

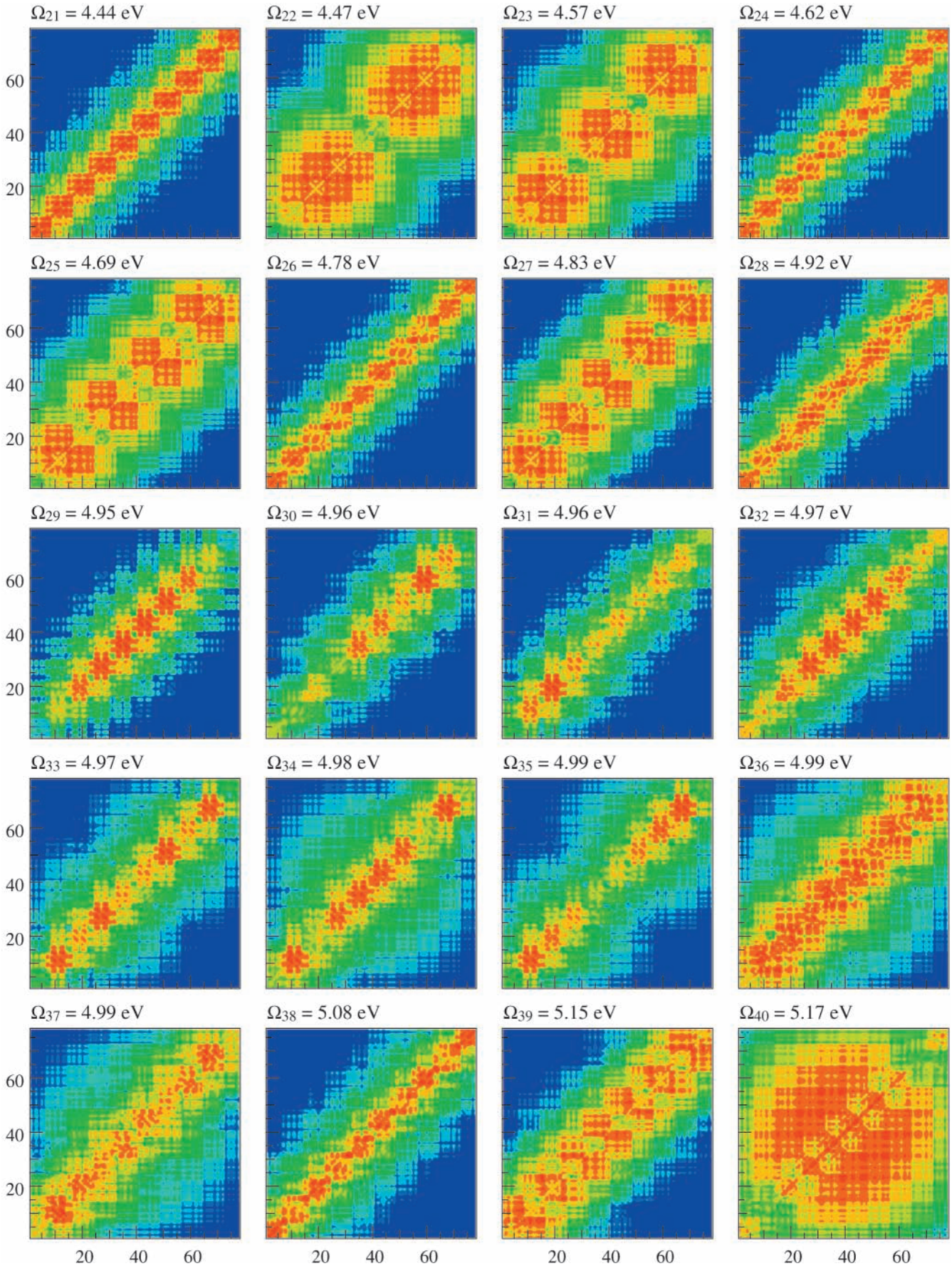

Figure 8 (continued)

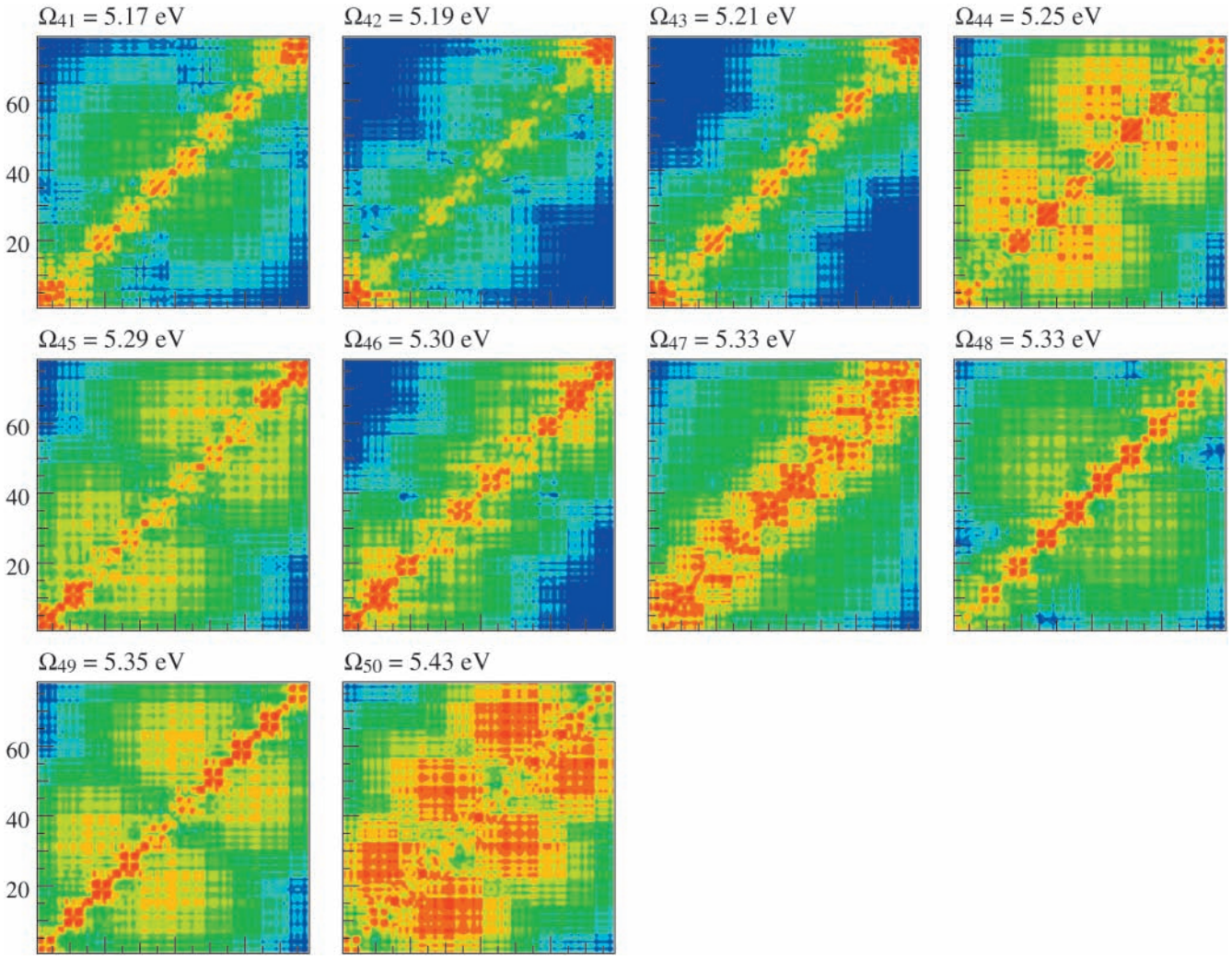

Figure 8 (continued)

alternation. The second factor is the square of the relative motion wave functions $g(n;s)$ of an exciton at the origin ($n = 0$) that depends parametrically on the center-of-mass momentum s. $I(\mathbf{q})$ thus contains indirect information on the dependence of the exciton size on its momentum. The first factor in eq 4.2 is a simple Lorentzian whose width is determined by the bond alternation parameter ζ. The deviation from the Lorentzian form provides the momentum dependence of the relative-motion exciton wave function when an electron and a hole occupy the same site ($n = 0$). Since the latter is directly related to the exciton size, the signal carries indirect information on the momentum dependence of the exciton size.

Acknowledgment. The support of the National Science Foundation and the Petroleum Research Fund administered by the American Chemical Society is gratefully acknowledged.

Appendix A: Density Response and the Structure Factor

We assume that the system is coupled to an external potential $E'(\tau)$ via an interaction Hamiltonian $\hat{H}'_{\text{int}}(\tau) = -E'(\tau)\hat{P}(\mathbf{q},\varphi)$ where $\hat{P}(\mathbf{q},\varphi)$ is an effective charge density operator that depends parametrically on the wavevector $\mathbf{q}$ and a phase φ:

$$\hat{P}(\mathbf{q},\varphi) = \hat{n}(\mathbf{q})e^{i\varphi} + \hat{n}(-\mathbf{q})e^{-i\varphi} \qquad \text{(A1)}$$

and $\hat{n}(\mathbf{q})$ is the Fourier transform of the electronic-density operator $\hat{n}(\mathbf{r})$ (eq 1.3). Note that $\hat{H}'_{\text{int}}(\tau)$ differs from that used in section II. Including φ allows us to manipulate the response and connect it with the structure factor. The corresponding time-domain linear response function $\bar{R}$ is defined by expanding the expectation value of the Heisenberg-picture operator $\tilde{n}(-\mathbf{q},\tau)e^{-i\varphi}$ in powers of the effective driving potential:

$$\langle\tilde{n}(-\mathbf{q},\tau)\rangle e^{-i\varphi} = \int_0^\infty dt\, \bar{R}(t;\mathbf{q},\varphi)E'(\tau - t) + \ldots \qquad \text{(A2)}$$

We further introduce a frequency-domain linear response function $\bar{\alpha}(\omega;\mathbf{q},\varphi)$ that also depends parametrically on $\mathbf{q}$ and φ:

$$\bar{\alpha}(\omega;\mathbf{q},\varphi) \equiv \int_0^\infty dt\, \bar{R}(t;\mathbf{q},\varphi)\exp(i\omega t) \qquad \text{(A3)}$$

The spectral decomposition of the linear response function $\bar{\alpha}(\omega;\mathbf{q},\varphi)$ is

$$\bar{\alpha}(\omega;\mathbf{q},\varphi) = \sum_\nu \frac{|\langle 0|\hat{n}(\mathbf{q})|\nu\rangle|^2}{\omega + \Omega_\nu + i\Gamma} - \sum_\nu \frac{|\langle \nu|\hat{n}(\mathbf{q})|0\rangle|^2}{\omega - \Omega_\nu + i\Gamma} + \sum_\nu \frac{\langle 0|\hat{n}(-\mathbf{q})|\nu\rangle\langle 0|\hat{n}(\mathbf{q})|\nu\rangle}{\omega + \Omega_\nu + i\Gamma}\exp(-2i\varphi) - \sum_\nu \frac{\langle 0|\hat{n}(-\mathbf{q})|\nu\rangle\langle 0|\hat{n}(\mathbf{q})|\nu\rangle}{\omega - \Omega_\nu + i\Gamma}\exp(2i\varphi) \qquad \text{(A4)}$$

the spectral decomposition of the dynamic structure factor (eq 1.2) gives

$$S(\mathbf{q},\omega) = \sum_{\upsilon} |\langle \upsilon|\hat{n}(\mathbf{q})|0\rangle|^2 \frac{2\Gamma}{(\omega - \Omega_{\upsilon})^2 + \Gamma^2} \qquad \text{(A5)}$$

where Γ is a relaxation rate. Comparing eqs A4 and A5 we obtain

$$S(\mathbf{q},\omega) = 2\int_0^{2\pi} \frac{d\varphi}{2\pi} \mathrm{Im}[\bar{\alpha}(\omega;\mathbf{q},\varphi)] \qquad \text{(A6)}$$

It follows immediately from eqs 2.1 and A1 that

$$\bar{\alpha}(\omega;\mathbf{q},\varphi) = \int d\mathbf{r}d\mathbf{r}'\alpha(\omega;\mathbf{r},\mathbf{r}')\{\exp[i\mathbf{q}\cdot(\mathbf{r}-\mathbf{r}')] + \exp[i\mathbf{q}\cdot(\mathbf{r}+\mathbf{r}') - 2i\varphi]\} \qquad \text{(A7)}$$

Substituting eq A7 into eq A6 we obtain eq 2.5.

Appendix B: Dynamical Structure Factor In Infinite 1D Lattices

In this appendix, we derive expressions for the dynamic structure factor of polymers of infinite length with 1D discrete translational symmetry. The generalization to 2D and 3D discrete translational symmetry is straightforward. We will rely on the INDO (intermediate neglect of differential overlap) approximation, without alluding to a specific Hamiltonian parametrization. For better numerical precision, one might want to use a higher-level approach, such as ab initio calculations described in refs 30−32. Various approaches that were successfully used for calculating polymer response were extensively analyzed and compared in ref 33, which included discussion of TDDFT computations in polymers and numerical convergence issues for different algorithms.

Each unit cell is represented by a basis set of K atomic orbitals $\varphi_m(\mathbf{r})$ (K is generally larger than the number of atoms in a unit cell). Introducing the annihilation (creation) operators $\hat{c}_{m,j}$ ($\hat{c}^+_{m,j}$) of an electron on the mth orbital in the jth unit cell, the Hamiltonian assumes the form:

$$\hat{H} = \sum t_{mn}(j)\hat{c}^+_{m,j'+j}\hat{c}_{n,j'} + \frac{1}{2}\sum U_{mnkl}(j)\hat{c}^+_{m,j'+j}\,\hat{c}^+_{n,j'}\hat{c}_{k,j'}\hat{c}_{l,j'+j} \qquad \text{(B1)}$$

where $t_{mn}(j)$ describe electron hopping from orbital n of unit cell j' to orbital m of unit cell $j'+j$. This matrix element is independent of j' because of translational symmetry. The Coulomb matrix elements in eq B1 are obtained by neglecting the overlaps of atomic orbitals on different atoms. This is known in quantum chemistry as the INDO approximation. The Hamiltonian parameters are, therefore, a j-dependent hopping matrix $t_{mn}(j)$ and tetradic Coulomb matrix $U_{mnkl}(j)$. The ground-state density matrix $\bar{\rho}_{m,j'+j;n,j'}$ is translationally invariant as well and can be represented as

$$\bar{\rho}_{m,j'+j;n,j'} = \bar{\rho}_{mn;j} \qquad \text{(B2)}$$

Here $\bar{\rho}_{mn;j}$ is a matrix-valued function of an integer argument j (a j-dependent matrix). Translational symmetry also implies that each eigenmode of eq 2.6 has a circular momentum s with $s + 2\pi = s$ and is expressed in terms of a j-dependent matrix $\tilde{\xi}_{mn,j}$:

$$\xi_{m,j'+j;n,j'}(s) = \exp(isj')\tilde{\xi}_{mn;j}(s) \qquad \text{(B3)}$$

The modes are, therefore, represented by j-dependent matrixes $\tilde{\xi}^{(\upsilon)}(s)$ that depend parametrically on the momentum s, and υ labels the modes for a given momentum. Using this notation, eq 2.6 adopts the form:

$$L(s)\tilde{\xi}^{(\upsilon)}(s) = \Omega^{(\upsilon)}(s)\tilde{\xi}^{(\upsilon)}(s) \qquad \text{(B4)}$$

where the operator $L(s)$ acts in the space of j-dependent matrixes $\tilde{\xi}_{mn;j}$. Substituting eqs B2 and B3 into eq 2.6 yields, after some straightforward transformations:

$$L(s)\tilde{\xi} = [h,\tilde{\xi}]_s + [\tilde{\rho},V(s)\tilde{\xi}]_s \qquad \text{(B5)}$$

In eq B5, we have introduced the deformed commutator:

$$([\tilde{\xi},\tilde{\eta}]_s)_{mn;j} \equiv \sum_{n',k}(\tilde{\xi}_{mn';j-k}\tilde{\eta}_{n'n;k} - \exp[is(j-k)]\tilde{\eta}_{mn';k}\tilde{\xi}_{n'n;j-k}) \qquad \text{(B6)}$$

$V(s)$ is an operator acting in the space of j-dependent matrixes that further depend parametrically on s:

$$[V(s)\tilde{\xi}]_{mn;j} = \sum_{m'n'}[\delta_{0j}\bar{U}_{mn'nm'}(s) - U_{mn'nm'}(j)]\tilde{\xi}_{m'n';j} \qquad \text{(B7)}$$

$\bar{U}_{mnkl}(s)$ is a Fourier transform of $U_{mnkl}(j)$:

$$\bar{U}_{mnkl}(s) = \sum_j U_{mnkl}(j)\exp(-isj) \qquad \text{(B8)}$$

h is an analogue of the Fock matrix:

$$h = \tilde{t} + V(0)\tilde{\rho} \qquad \text{(B9)}$$

where $\tilde{t}_{mn;j} \equiv t_{mn}(j)$. We have also chosen the coefficients $U_{mnkl}(j)$ such that

$$U_{nmlk}(-j) = U_{mnkl}(j) \qquad \text{(B10)}$$

Using the above notation, we can recast eq 2.9 for the dynamic structure factor $S(\mathbf{q},\omega)$ in the form of eq 2.11. We further need to introduce a Bloch function $\tilde{\mu}(\mathbf{q})$ for the Fourier transform of the electronic-density function, which is defined similarly to eq B3:

$$\bar{\mu}_{m,j'+j;n,j'}(\mathbf{q}) = \exp[-i(\mathbf{q}\cdot\mathbf{R})j']\,\tilde{\mu}_{mn;j}(\mathbf{q}) \qquad \text{(B11)}$$

where $\bar{\mu}(\mathbf{q})$ is given by eq 2.10 except that each atomic orbital is labeled by two indices m and j (rather than one). It is easy to see from eqs 2.10 and B11 that if we neglect the overlap of orbitals belonging to different atoms then $\tilde{\mu}_{mn;j}(\mathbf{q}) \propto \delta_{0j}$, consequently, we only need to know $\bar{\mu}(\mathbf{q})$ within the 0th unit cell of the polymer.

The normalization of the modes in a translationally invariant polymer adopts a form:

$$\mathrm{Tr}\{\tilde{\xi}^{(\mu)\dagger}(s)[\bar{\rho},\tilde{\xi}^{(\upsilon)}(s')]\} = -2\pi\,\mathrm{sgn}(\Omega^{(\upsilon)}(s))\delta_{\mu\upsilon}\delta(s-s') \qquad \text{(B12)}$$

This immediately yields for the positive-frequency modes:

$$\sum_{mn,j}\tilde{\xi}^{(\mu*)}_{mn;j}(s)\,([\tilde{\rho},\tilde{\xi}^{(\upsilon)}(s)]_s)_{mn;j} = -\mathrm{sgn}(\Omega^{(\upsilon)}(s))\delta_{\mu\upsilon} \qquad \text{(B13)}$$

With the $\tilde{\xi}^{(\upsilon)}$ and $\Omega^{(\upsilon)}$ found from eq B4, $\tilde{\xi}^{(\upsilon)}$ being normalized according to eq B13, and with $\tilde{\mu}(\mathbf{q})$ defined by eqs B11 and

2.10, we can calculate the dynamic structure factor given by eq 2.11.

Appendix C: Linearized TDHF Equation in Infinite Chains: Molecular-Orbital Representation

In this appendix, we recast the linearized TDHF equation (eqs 2.6 and B5) in infinite chains using the molecular orbitals basis set. We start with the Bloch representation of orbitals:

$$\bar{\psi}_{m,j;\alpha}(s) = \exp(isj)\psi_{m\alpha}(s) \tag{C1}$$

where α parametrize molecular orbitals with momentum s. The molecular orbitals are the eigenstates of the single-particle Hartree−Fock Hamiltonian $h_{mn;j}$ introduced in eq B9:

$$\sum_n \bar{h}_{mn}(s)\psi_{n\alpha}(s) = \epsilon_\alpha(s)\psi_{m\alpha}(s) \tag{C2}$$

where $\bar{h}_{mn}(s)$ is the Fourier transform of $h_{mn;j}$:

$$\bar{h}_{mn}(s) \equiv \sum_j h_{mn;j} \exp(-isj) \tag{C3}$$

The CEO modes $\tilde{\xi}_{mn;j}$ may be recast using the molecular orbitals:

$$\tilde{\xi}_{mn;j}(s) = \sum_{\alpha\beta} \int \frac{ds'}{2\pi} \psi_{m\alpha}(s')\psi^*_{n\beta}(s'-s) f_{\alpha\beta}(s';s) \exp(is'j) \tag{C4}$$

Equation C4 represents a CEO mode with parametric dependence on momentum s as a superposition of contributions whereby an electron from orbital β with the momentum $s'-s$ is moved to orbital α and momentum s'.

The inverse transformation [i.e., from $\tilde{\xi}$ to $f(s)$] has a form

$$f_{\alpha\beta}(s';s) = \sum_j \sum_{mn} \psi^*_{m\alpha}(s')\psi_{n\beta}(s'-s)\tilde{\xi}_{mn;j}(s) \exp(-is'j) \tag{C5}$$

We further introduce the function $\mathrm{sgn}(\alpha) \equiv 1(-1)$ if the orbital α is occupied (unoccupied).

The operator $L(s)$ in the molecular-orbital representation is obtained by substituting eqs C4 and C5 into eq B5 and making use of eq C2 which yields:

$$L(s)f_{\alpha\beta}(s'';s) = [\epsilon_\alpha(s'') - \epsilon_\beta(s''-s)]f_{\alpha\beta}(s'';s) - [\mathrm{sgn}(\alpha) - \mathrm{sgn}(\beta)] \sum_{\alpha'\beta'} \int \frac{ds'}{2\pi} [\bar{V}_{\alpha\beta\alpha'\beta'}(s'',s';s) - \bar{V}_{\alpha\alpha'\beta\beta'}(s'',s''-s;s''-s')]f_{\alpha'\beta'}(s';s) \tag{C6}$$

where we have used the matrix elements of the Coulomb interaction in the molecular orbitals basis set:

$$\bar{V}_{\alpha\beta\alpha'\beta'}(s'',s';s) \equiv \sum_{mnm'n'} \bar{U}_{mnm'n'}(s''-s')\psi_{m'\alpha'}(s')\psi^*_{n'\beta'}(s'-s) \times \psi^*_{m\alpha}(s'')\psi_{n\beta}(s''-s) \tag{C7}$$

Since the modes do not have intraband components, $f_{\alpha\beta}(s';s) \neq 0$ only if $\mathrm{sgn}(\alpha) \neq \mathrm{sgn}(\beta)$.

The expressions for the Hartree−Fock Hamiltonian (eq C2) and for the Liouville operator (eqs C6 and C7) written in the molecular orbital representation will be further used in Appendix D for studying a model of an infinite periodic molecule.

Appendix D: Signatures of Exciton Sizes in EELS Spectroscopy

In this appendix, we consider a simple model of an infinite polymer chain with two orbitals per unit cell and a Pariser−Parr−Pople (PPP) type Hamiltonian. This model will be used in section IV to establish some qualitative analytical criteria for the possibility of extracting exciton size information from EELS measurements. Higher level computations on polymers can be found in ref 34. We will analyze the limit of weak bond alteration whereby the bond alternation parameter $\zeta \ll 1$. It will be instructive to consider the case of weak Coulomb interaction when the exciton size $l_e \gg \zeta^{-1}$ where the analysis can be made analytically. The molecular-orbital representation of the linearized TDHF equation will be used here, which is described in Appendix C.

We first note that in this case we can neglect the Coulomb contribution to the single-electron Hamiltonian h. Assuming nearest-neighbor hopping, we have the following nonzero elements of h:

$$h_{12;0} = h_{21;0} = \left(1 - \frac{\zeta}{2}\right)t$$
$$h_{12;1} = h_{21;-1} = \left(1 + \frac{\zeta}{2}\right)t \tag{D1}$$

where t is the average hopping and $\zeta \ll 1$ is the bond alternation parameter. Equation D1 yields for $\bar{h}(s)$ defined by eq C3

$$\bar{h}_{12}(s) = \bar{h}^*_{21}(s) = \left[\left(1 - \frac{\zeta}{2}\right) + \left(1 + \frac{\zeta}{2}\right)\exp(-is)\right]t \tag{D2}$$

Denoting the upper (lower) electron bands by $+(-)$ we obtain upon the substituting of eq D2 into eq C2

$$\epsilon_\pm(s) = \pm t[\zeta^2 + 2(1-\zeta^2)(1+\cos s)]^{1/2} \tag{D3}$$

and

$$\psi_{1\pm}(s) = \frac{1}{\sqrt{2}\epsilon_\pm(s)}\bar{h}_{12}(s), \quad \psi_{2\pm}(s) = \frac{1}{\sqrt{2}} \tag{D4}$$

We will show later that the relevant momenta in the problem are $s - \zeta$. Equations D3 and D4 then adopt the form:

$$\epsilon_\pm(s) = \pm t(\zeta^2 + s^2)^{1/2}$$
$$\psi_{1\pm}(s) = \pm \frac{-\zeta + is}{\sqrt{2}(\zeta^2 + s^2)^{1/2}} \tag{D5}$$

Consider now a CEO mode with positive frequency Ω. It is determined by a pair of function $f_{+-}(s';s)$ and $f_{-+}(s';s)$ where the operator $L(s)$ is given by eq C6. When the Coulomb interaction is weak, we can neglect $f_{-+}(s';s)$ in the equation for a positive frequency eigenmode. Denoting $f_+(s';s) \equiv f_{+-}(s';s)$, we obtain the normalization

$$\int_{-\pi}^{\pi} \frac{ds'}{2\pi} |f_+(s';s)|^2 = 1 \tag{D6}$$

We now find the value of s' for which the kinetic energy $\epsilon_+(s') - \epsilon_-(s'-s)$ of an electron−hole pair has a minimum:

$$\frac{d}{ds'}[\epsilon_+(s') + \epsilon_+(s'-s)] = 0 \qquad \text{(D7)}$$

When s is not too large (i.e., $s \sim \zeta$) this yields $s'_0 = s/2$. We then look for the solution of the eigenmode in a form

$$f_+(s';s) = \bar{f}(s'-s;s) \qquad \text{(D8)}$$

where $\bar{f}(s';s)$ is substantially nonzero for $|s'| \sim l_e^{-1} \ll |s| \sim \zeta$.

Substituting eq D8 into eq C6 and neglecting the momentum dependence of $\psi_{m\alpha}(\tilde{s})$ in eq C7 (i.e., setting $s' = s'' = s/2$ in ψ when computing $\bar{V}$ in eq C6 using eq C7) yields:

$$[\epsilon_e(s';s) - \Omega]\bar{f}(s';s) + \int \frac{ds''}{2\pi}\bar{V}^{(0)}(s''-s';s)\,\bar{f}(s'';s) + \bar{V}^{(1)}(s)\int \frac{ds''}{2\pi}\bar{f}(s'';s) = 0 \qquad \text{(D9)}$$

where

$$\epsilon_e(s';s) \equiv \epsilon_+\left(\frac{s}{2}+s'\right) + \epsilon_+\left(-\frac{s}{2}+s'\right)$$

$$\bar{V}^{(0)}(s';s) \equiv -\sum \bar{U}_{mnm'n'}(2s')\psi_{m'+}\left(\frac{s}{2}\right)\psi^*_{n'-}\left(-\frac{s}{2}\right)\psi^*_{m+}\left(\frac{s}{2}\right)\psi_{n-}\left(-\frac{s}{2}\right) \qquad \text{(D10)}$$

$$\bar{V}^{(1)}(s) \equiv \sum \bar{U}_{mnm'n'}(s)\,\psi_{m'+}\left(\frac{s}{2}\right)\psi^*_{n'-}\left(-\frac{s}{2}\right)\psi^*_{m+}\left(\frac{s}{2}\right)\psi_{n-}\left(-\frac{s}{2}\right)$$

Note that for small s' we have $\bar{V}^{(0)}(s';s) \sim \ln|s'|$ and $V^{(1)}(s)$ has a finite value at $s \to 0$. For relevant values of s' we also have

$$\epsilon_e(s';s) = \epsilon_0(s) + \frac{1}{2}m_{\text{eff}}^{-1}(s)(s')^2 \qquad \text{(D11)}$$

with the s-dependent exciton mass

$$m_{\text{eff}}^{-1}(s) = \frac{[\zeta^2 + (s/2)^2]^{3/2}}{\zeta^2} \qquad \text{(D12)}$$

Equation D9 may be solved by introducing the Fourier transform $g(n;s)$ of $\bar{f}(s';s)$:

$$g(n;s) \equiv \int \frac{ds'}{2\pi}\,\bar{f}(s';s)\exp(is'n) \qquad \text{(D13)}$$

It then adopts a form:

$$\frac{1}{2}J(s)[g(n+1;s) + g(n-1;s)] - \Omega(s)g(n;s) + V^{(0)}(n;s)g(n;s) + \bar{V}^{(1)}(s)\delta_{n,0}\,g(0;s) = 0 \qquad \text{(D14)}$$

with

$$V^{(0)}(n;s) \equiv \int \frac{ds'}{2\pi}\,\bar{V}^{(0)}(s';s)\exp(is'n) \qquad \text{(D15)}$$

and

$$J(s) = [m_{\text{eff}}(s)]^{-1} \qquad \text{(D16)}$$

The eigenvalue problem eq D14 is equivalent to a 1D particle on a lattice with potential $V^{(0)}(n;s) + \bar{V}^{(1)}(s)\delta_{0n}$. The structure factor $S(\mathbf{q},\omega)$ assumes the following form:

$$S(\mathbf{q},\omega) = \frac{2\Gamma}{[\omega - \Omega(\mathbf{q}\cdot\mathbf{R})]^2 + \Gamma^2}A(\mathbf{q}\cdot\mathbf{R})|g(0;\mathbf{q}\cdot\mathbf{R})|^2 \qquad \text{(D17)}$$

where

$$A(s) = |\psi^*_{1+}(s)\psi_{1-}(s) + \psi^*_{2+}(s)\psi_{2-}(s)|^2 \qquad \text{(D18)}$$

It follows from eq D5 that for the relevant momentum

$$A(s) = \frac{s^2}{\zeta^2 + s^2} \qquad \text{(D19)}$$

Equations D17, D19, and D14 describe the momentum dependence of the dynamic structure factor $S(\mathbf{q},\omega)$.

References and Notes

(1) Mukamel, S. *Principles of Nonlinear Optical Spectroscopy*; Oxford University Press: New York, 1995.

(2) *Time-Resolved Diffraction*; Helliwell, J. R., Rentzepis, P. M., Eds.; Oxford University Press: New York, 1997.

(3) Steinmeyer, G.; Sutter, D. H.; Gallmann, L.; Matuschek, N.; Keller, U. *Science* **1999**, *286*, 1507.

(4) Schoenlein, R. W.; Chattopadhyay, S.; Chong, H. H. W.; et al. *Science* **2000**, *287*, 223.

(5) Rehr, J. J.; Albers, R. C. *Rev. Mod. Phys.* **2000**, *72*, 621.

(6) Brown, F.; Wilson, K.; Cao, J. *J. Chem. Phys.* **1999**, *111*, 6238.

(7) Tomov, I. V.; Oulianov, D. A.; Chen, P.; Rentzepis, P. M. *J. Phys. Chem. B* **1999**, *103*, 7081.

(8) Åberg, T.; Crasemann, B. In *X-ray Resonant Scattering*; Materlik, G., Fischer, K., Sparks, C., Eds.; Elsevier: New York, 1993.

(9) Williamson, J. C.; Cao, J.; Ihee, H.; Frey, H.; Zewail, A. H. *Nature (London)* **1997**, *386*, 159.

(10) Williamson, J. C.; Zewail, A. H. *J. Phys. Chem.* **1994**, *98*, 2766.

(11) Ben-Nun, M.; Martinez, T. J.; Weber, P. M.; Wilson, K. R. *Chem. Phys. Lett.* **1996**, *262*, 405.

(12) Elsayed-Ali, H. E.; Weber, P. M. In *Time-Resolved Diffraction*; Helliwell, J. R., Rentzepis, P. M., Eds.; Oxford University Press: New York, 1997; p 284.

(13) Parker, S. F.; Braden, D. A.; Tomkinson, J.; Hudson, B. *J. Phys. Chem. B* **1998**, *102*, 5955.

(14) Fink, J. *Transmission Electron Energy Loss Spectroscopy*, in *Topics in Applied Physics*, Vol. 69, Fuggle, J. C., Inglesfield, J. E., Eds.; Springer-Verlag: New York, 1992; p 203.

(15) Knupfer, M.; Pichler, T.; Golden, M. S.; et al. *Phys. Rev. Lett.* **1999**, *83*, 1443.

(16) Knupfer, M.; Fink, J.; Zojer, E.; Leising, G.; Brédas, J. L. *Phys. Rev. B* **2000**, *61*, 1662.

(17) Knupfer, M.; Fink, J.; Zojer, E.; Leising, G.; Fichou, D. *Chem. Phys. Lett.* **2000**, *318*, 585.

(18) Ring, P.; Schuck, P. *The Nuclear Many-Body Problem*; Springer-Verlag: New York, 1976.

(19) Chernyak, V.; Mukamel, S. *J. Chem. Phys.* **1996**, *104*, 444.

(20) Mukamel, S.; Tretiak, S.; Wagersreiter, T.; Chernyak, V. *Science* **1997**, *277*, 781; Tretiak, S.; Chernyak, V.; Mukamel, S. *J. Am. Chem. Soc.* **1997**, *119*, 11408.

(21) Chernyak, V.; Mukamel, S. *J. Chem. Phys.* **2000**, *112*, 3572.

(22) Pellegrin, E.; Fink, J.; Drechsler, S. L. *Phys. Rev. Lett.* **1991**, *66*, 2022.

(23) Zojer, E.; Knupfer, M.; Resel, R.; et al., *Phys. Rev. B* **1997**, *56*, 10138.

(24) Frisch, M. J., et al., Gaussian94; Gaussian, Inc., Pittsburgh, 1995.

(25) Ridley, J.; Zerner, M. C. *Theor. Chim. Acta* **1973**, *32*, 111.

(26) Zerner, M. C.; Loew, C. H.; Kirchner, R. F.; Mueller-Westerhoff, U. T. *J. Am. Chem. Soc.* **1980**, *102*, 589.

(27) Chernyak, V.; Schulz, M.; Mukamel, S.; Tretiak, S.; Tsiper, E. *J. Chem. Phys.* **2000**, *113*, 36.

(28) Chernyak, V.; Volkov, S. N.; Mukamel, S. *Phys. Rev. Lett.* **2001**, *86*, 995.

(29) Zyss, J.; Ledoux, I.; Volkov, S. N.; Chernyak, V.; Mukamel, S. *J. Am. Chem. Soc.* **2000**, *122*, 11956.

(30) Vračko, M. G.; Zaider, M. *Int. J. Quantum Chem.* **1993**, *47*, 119.

(31) Vračko, M. G.; Champagne, B.; Mosley, D. H.; André, J.-M. *J. Chem. Phys.* **1995**, *102*, 6831.

(32) Vračko, M. G.; Zaider, M. *Int. J. Quantum Chem.* **1992**, *43*, 321.

(33) Hirata, S.; Head-Gordon, M.; Bartlett, R. J. *J. Chem. Phys.* **1999**, *111*, 10774.

(34) Champagne, B.; Fripiat, J. G.; André, J.-M. *J. Chem. Phys.* **1992**, *96*, 8330.